Hyperfine structure of the ground state of para-D_2^+ by high-resolution Rydberg-state spectroscopy and multichannel quantum defect theory

H. A. Cruse,[1] Ch. Jungen,[2] and F. Merkt[1]

[1]*Laboratorium für Physikalische Chemie, ETH Zurich, 8093 Zurich, Switzerland*

[2]*Laboratoire Aimé Cotton, CNRS II, Bâtiment 505, Campus d'Orsay, 91405 Orsay Cedex, France*

(Received 22 January 2008; published 1 April 2008)

The hyperfine structure of transitions between $n=51-53d$ and $n=54-57f$ Rydberg states belonging to series converging on the $X\ ^2\Sigma_g^+$ ($v^+=0$, $N^+=1$), ground state of para-D_2^+ has been measured at an experimental resolution of about 1 MHz by millimeter-wave spectroscopy and assigned on the basis of combination differences. A map of the hyperfine structure of these Rydberg states has been determined. The analysis of the hyperfine structure of the nf series by multichannel quantum defect theory has confirmed the experimental assignments and enabled the derivation of the hyperfine structure of the ground state of para-D_2^+ with a precision of better than 1 MHz.

I. INTRODUCTION

Studies of molecular Rydberg states by high-resolution spectroscopy provide information on their structure and dynamics [1–7]. Rydberg spectra consist of long progressions of spectral features which converge to ionization thresholds. The Rydberg series below, and the continua above the ionization thresholds form what are called ionization channels. Scaling laws describing the properties of Rydberg states as a function of the principal quantum number n, and the continuity of these properties as the ionization thresholds are crossed, enable one to derive information on molecular photoionization dynamics and on the energy level structure of molecular cations from high-resolution spectra of Rydberg states.

Multichannel quantum defect theory (MQDT) represents the ideal tool with which to describe ionization channels [8–10]. The theory treats the Rydberg series and the adjoining continua in a unified manner in terms of the scattering of the excited electron with the positively charged ion core. The quantum defect parameters, derived either by *ab initio* theory or from experiments, include quantum defect functions that depend on the electron energy and the geometrical structure of the molecular cation and provide, at least in principle, a complete description of the photoionization dynamics. The theory can be used to treat dissociation and ionization in a unified manner [11–14] and to incorporate the effects of nuclear spins in atomic [15–17] and molecular [18,19] photoionization.

The Rydberg and photoionization spectra of molecular hydrogen have played an important role in the development and testing of molecular MQDT [6,7,9,12–14,18,20–22]. In recent studies of bound np and nf Rydberg states of H_2 below the $X\ ^2\Sigma_g^+$ ($v^+=0$, $N^+=1$) ground state [18] and of np autoionizing Rydberg series converging to the first excited rotational level ($N^+=3$) [19] of ortho-H_2^+ we found the combination of high-resolution spectroscopy and MQDT to be well suited for studying the hyperfine structure of high Rydberg states and investigating how nuclear spins influence the molecular photoionization dynamics. Moreover, the extrapolation, by MQDT, of the Rydberg series led to the determi-

nation of the hyperfine structure of the ground state of ortho-H_2^+.

The present paper summarizes the results of an investigation of the hyperfine structure of high Rydberg states of para-D_2 by millimeter-wave spectroscopy and MQDT from which the hyperfine structure of the ground state of para-D_2^+ could be determined for the first time. The experimental and theoretical methodologies used to record and analyze the spectra are the same as those used in our previous investigation of the Rydberg states of ortho-H_2^+ and are described in detail in Ref. [18]. They are therefore only succinctly summarized in Secs. II and IV. The experimental methodology relies on the measurement of millimeter-wave spectra of transitions between neighboring long-lived Rydberg states. In the preparatory phase of the present experiments, the long-lived ns and nd Rydberg states of para-D_2 below the ionization threshold, which are needed as initial states for the millimeter-wave transitions, were identified by laser spectroscopy and pulsed field ionization techniques [23]. The theoretical methodology relies on accurate quantum defect functions determined *ab initio* and refined in fits to high-resolution spectroscopic data [18].

II. EXPERIMENT

nd Rydberg states of D_2 converging on the $X\ ^2\Sigma_g^+$ ($v^+=0$, $N^+=1$), threshold were accessed using the double-resonance excitation scheme illustrated in Fig. 1. Para-D_2 ($I=1$) was selected by exciting the $R(1)$ transition from the $X\ ^1\Sigma_g^+$ ($v''=0$) ground state to the $B\ ^1\Sigma_u^+$ ($v'=3$) state. Excitation via a vibrationally excited level of the B state was employed because the Franck-Condon overlap between X ($v''=0$) and B (v') states increases rapidly with v' [24].

Three pulsed dye lasers (Lambda Physik, Scanmate) pumped by the 532 nm or 355 nm output of a single Nd:YAG (YAG=yttrium aluminum garnet) laser (Quantel, repetition rate 16.7 Hz, pulse length 10 ns) were needed for the excitation process. The vacuum ultraviolet (vuv) radiation, of wave number $\tilde{\nu}_{vuv}=2\tilde{\nu}_1+\tilde{\nu}_2$, required for the $B(v'=3)\leftarrow X(v''=0)$ $R(1)$ transition was generated by resonance-
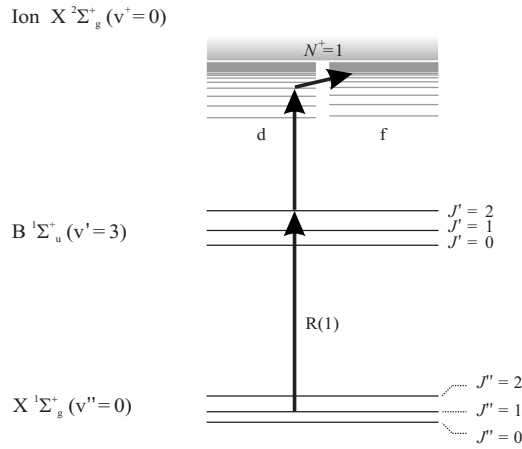
FIG. 1. Excitation scheme used to study the hyperfine structure of nd and nf Rydberg states located below the $X\,^2\Sigma_g^+$ ($v^+=0$, $N^+=1$) ground state of para-D_2^+.

enhanced sum-frequency mixing in a xenon jet of the doubled output of the first dye laser [355 nm pump, $2\tilde{\nu}_1 = 80\,118.98$ cm^{-1}, corresponding to the $5p^5(^2P_{3/2})5p[1/2](J=0)\leftarrow4p^6\,^1S_0$ two-photon transition of atomic xenon] and the near ir output of the second dye laser (532 nm pump, Pyridine 2, $\tilde{\nu}_2=13278.0$ cm^{-1}). The doubled output of the third dye laser (532 nm pump, $\tilde{\nu}_3 \approx 31250$ cm^{-1}) was used to excite transitions from the B ($v'=3, J'=2$) state to nd Rydberg states with principal quantum number n between 51 and 53 located below the $X\,^2\Sigma_g^+$ ($v^+=0, N^+=1$) threshold of D_2. The dye laser wave numbers were calibrated during scans by simultaneous measurement of the optogalvanic spectrum of neon and comparison with tabulated transition wave numbers [25,26].

The vuv and uv laser beams were reflected into the photoexcitation chamber with perpendicular relative polarizations and intersected a pulsed skimmed supersonic beam of neat D_2 (99.8% purity, PanGas) on the axis of a set of six cylindrically symmetrical extraction plates. During operation of the pulsed valve (General Valve) the background pressure in the photoexcitation region was 5×10^{-7} mbar. The vuv, uv, and gas beams lay in a plane orthogonal to the time-of-flight axis; the vuv radiation propagated orthogonal to the gas beam and at an angle of 45° relative to the uv laser beam.

Transitions from the $51-53d$ Rydberg states to $54-57f$ Rydberg states were excited using millimeter waves produced by a frequency- and phase-stabilized backward-wave-oscillator-based synthesizer (AMC Chemnitz) operating in continuous mode. Frequencies between 120 GHz and 180 GHz could be generated and the frequency output was locked to a high harmonic of a microwave reference frequency. A parabolic mirror was used to weakly focus the millimeter-wave radiation into the excitation region, antiparallel to the vuv radiation. When necessary, a small voltage was applied across the stack of resistively coupled extraction plates within the chamber to compensate for stray electric fields, which can shift the observed millimeter-wave transition frequencies. The stray electric field was measured at regular intervals and compensated according to the method described in Ref. [27] to a level below 3 mV/cm^{-1}. The f
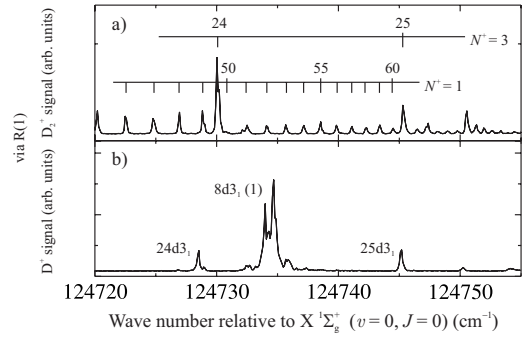

FIG. 2. Laser spectra of para-D_2 in the vicinity of the $X\,^2\Sigma_g^+$ ($v^+=0$, $N^+=1$) ionization threshold recorded via the $B\,^1\Sigma_u^+$ ($v'=3$, $J'=2$) intermediate state. (a) D_2^+ ion signal resulting from the pulsed field ionization of long-lived Rydberg states. (b) D^+ signal resulting from predissociation into a ground state D atom and a D atom in the $n=2$ state and subsequent photoionization of the D($n=2$) fragment during the 10-ns-long laser pulse. The "(1)" after $8d3_1$ indicates that the Rydberg level belongs to a $v^+=1$ series.

Rydberg states were field ionized by applying a voltage pulse of 1 μs duration to the extraction plates. The magnitude of the resulting electric field was carefully adjusted so as to minimize the field ionization of the d Rydberg states. This field also served to accelerate the resulting ions toward a multichannel plate detector. The delay between photoexcitation and pulsed-field ionization was chosen to be as long as possible so as to maximize the length of the interaction between the millimeter waves and the Rydberg states and obtain the best possible energy resolution. The delay time employed in the experiments described below resulted in a spectral resolution of 1 MHz. When necessary, the millimeter-wave radiation was attenuated to reduce power broadening by using an adjustable attenuator mounted to the source output. The signal-to-noise ratio in the millimeter-wave spectra was enhanced by repeating scans over the same region typically 5 times and averaging the results. Sets of spectra with common initial or final states were recorded to enable the assignment of the spectra by the method of combination differences (see Ref. [18] for more details).

III. EXPERIMENTAL RESULTS

An overview laser spectrum showing the initial d states used in this study is displayed in Fig. 2. The spectrum was recorded in a two-photon excitation sequence via the $B\,^1\Sigma_u^+$ ($v'=3$, $J'=2$) intermediate state. The D_2^+ ion signal resulting from the pulsed field ionization of long-lived Rydberg states is displayed in panel (a) and the D^+ signal resulting from predissociation into a ground state D atom and a D atom in the $n=2$ state followed by photoionization of the D($n=2$) fragment during the 10-ns-long laser pulse in panel (b). In Fig. 2, an intense Rydberg series converging on the ($v^+=0$, $N^+=1$) threshold of D_2^+ is observed, and only a few rotational or vibrational perturbing states are present.

Neglecting spin, the initial d states can be labeled using Hund's case d nomenclature, $n\ell N^+_N$, where ℓ is the Rydberg orbital angular-momentum quantum number, $\mathbf{N}^+$ is the total
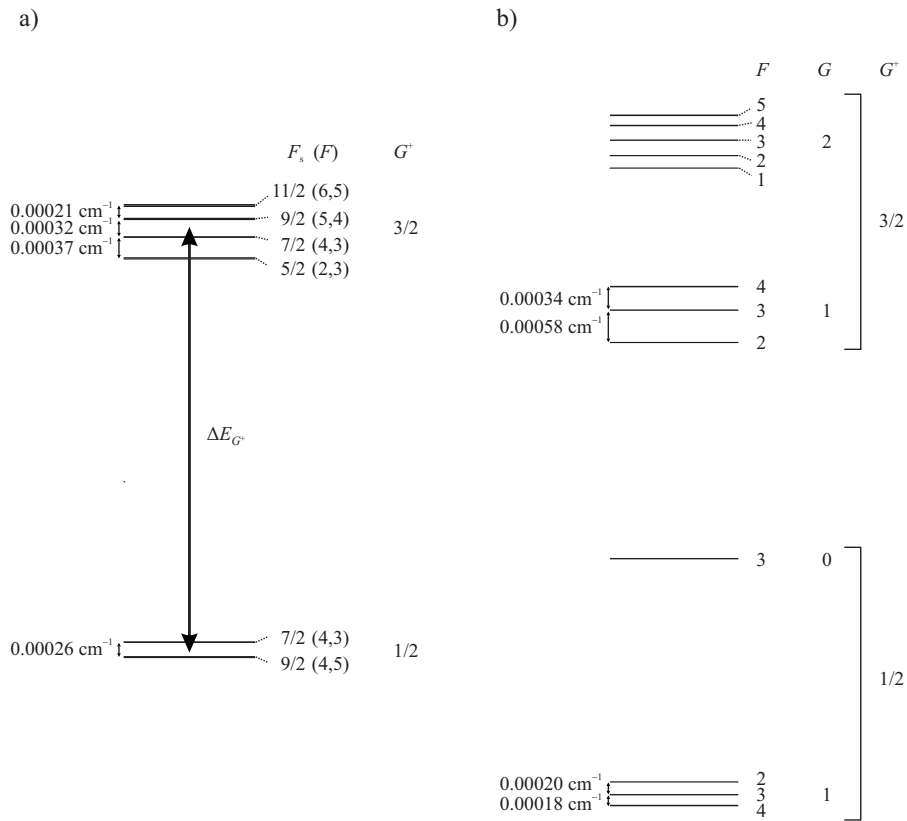
a)

b)

FIG. 3. Hyperfine structure of the $56f1_4$ [panel (a)] and $52d1_3$ [panel (b)] Rydberg states below the $X\,^2\Sigma_g^+$ $(v^+=0,\ N^+=1)$ ground state of para-D₂⁺. The nomenclature used to designate the hyperfine levels of the nd and nf Rydberg states differs and is explained in the text.

core angular momentum without spin, and **N** is the total angular momentum without spin. From the $(J'=2)$ level of the B state, the $ns1_1$, $nd1_1$, $nd1_2$, and $nd1_3$ Rydberg series converging on the $(v^+=0,\ N^+=1)$ threshold of D₂⁺ are accessible. At our laser resolution of 0.15 cm⁻¹ these series are not resolved, but an extensive survey of the s and d Rydberg states of para-D₂ using high-resolution home-built laser systems (0.01 cm⁻¹ resolution) was carried out by our group prior to the current work [23]. These high-resolution laser spectra and associated MQDT calculations revealed that the $ns1_1$ series is very weak, the $nd1_1$ series is absent, and the $nd1_2$ series is metastable but weak. The $nd1_3$ series is not as long lived as the $nd1_2$ series, but is by far the most intense series in the region of interest [23]. Therefore, only transitions originating from $nd1_3$ Rydberg states were observed in the millimeter-wave spectra and the accessible final states were thus limited to the $np1_2$, $nf1_2$, $nf1_3$, and $nf1_4$ Rydberg states.

The hyperfine coupling in D₂⁺ is predicted to be weaker than in H₂⁺ [28], and as a result, the hyperfine structure of the D₂⁺ ion is more dense than that of H₂⁺. In particular, the principal hyperfine splitting in the D₂⁺ ion is approximately 200 MHz, as compared to 1300 MHz in H₂⁺. Therefore, the onset of hyperfine-induced singlet-triplet mixing in the Rydberg states of D₂ occurs at higher principal quantum numbers than in H₂.

The experimentally measured hyperfine structures of the $56f1_4$ and $52d1_3$ Rydberg states are displayed in panels (a) and (b) of Fig. 3, respectively. In the nonpenetrating f states, the hyperfine interaction in the D₂⁺ ion core is stronger than the exchange interaction between the Rydberg and core electrons. Consequently, the nf levels are of mixed singlet and triplet character and the level structure is similar to that of the D₂⁺ ion. Each hyperfine state is designated by a label of three quantum numbers $F_s(F)G^+$, where $\mathbf{F}_s$ is the total angular momentum without the Rydberg electron spin, $\mathbf{F}$ is the total angular momentum, and $\mathbf{G}^+=\mathbf{I}+\mathbf{S}^+$ is the total core spin angular momentum. The splitting ΔE_{G^+} between the two sets of G^+ levels $(G^+=1/2$ and $3/2)$ is almost identical to the principal hyperfine splitting of the $N^+=1$ rotational level of the D₂⁺ ion.

In the more penetrating d states, the exchange interaction between the Rydberg and core electrons is comparable in strength to the hyperfine interaction in the D₂⁺ ion core and, as a result, the singlet-triplet mixing is not complete. These states correspond to a situation intermediate between the angular-momentum coupling cases d_{β_S} and $d_{\beta_{S^+}}$, already discussed in Ref. [19] for the np Rydberg series of H₂ beyond $n=100$. F_s is no longer a good quantum number, and the hyperfine levels are best labeled by the good quantum numbers F, G (**G** is the total spin), and the approximately good quantum number G^+. nd levels with $G=1$ can be accessed using the current laser excitation scheme (see Fig. 1), as explained in Ref. [19]. The splitting between the two sets of $G=1$ levels varies with n but is approximately equal to the G^+ splitting in the f states [see Fig. 3(b)].

An overview of the millimeter-wave spectra recorded during this study is presented in Fig. 4. $\Delta n=n_f-n_i=+3$ or $+4$ transitions $(i=\text{initial},\ f=\text{final})$ originating from the $G=1$ hyperfine components of $n_id1_3[1/2,3/2]$ states with $n_i=51-53$ were observed. In principle, the n_ff1_{2-4} and n_fp1_2 Rydberg series are accessible from these initial states, but
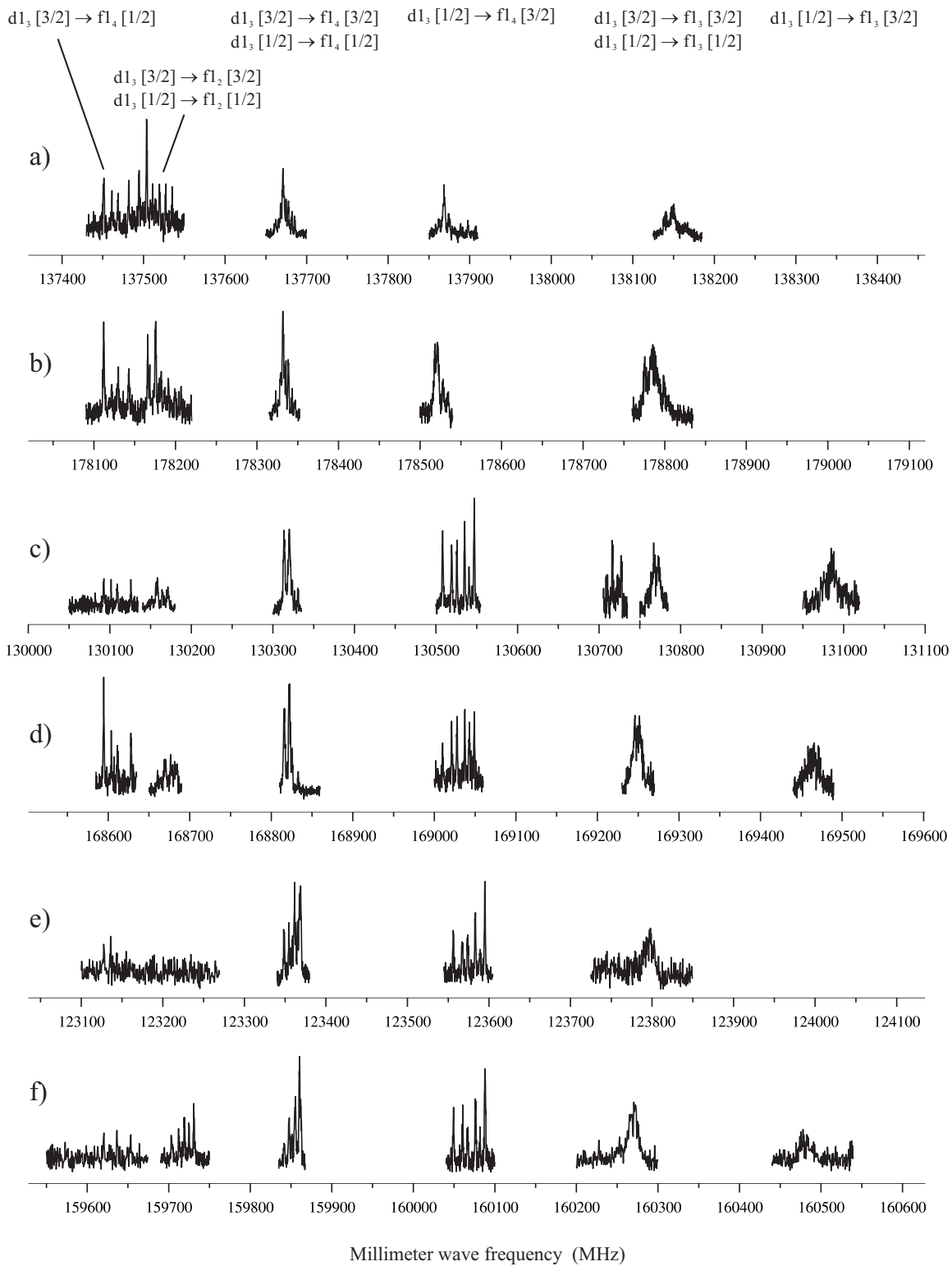
FIG. 4. Overview of the millimeter-wave spectra of transitions between nd and nf Rydberg states of para-D_2 located below the $X\ ^2\Sigma_g^+$ ($v^+=0$, $N^+=1$) ionization threshold. (a) $54f \leftarrow 51d$, (b) $55f \leftarrow 51d$, (c) $55f \leftarrow 52d$, (d) $56f \leftarrow 52d$, (e) $56f \leftarrow 53d$, (f) $57f \leftarrow 53d$. The spectral features are labeled $dN_N^+[G^+] \rightarrow fN_{N'}^+[G^{+\prime}]$.

scans of extended frequency regions did not reveal sharp lines at the positions expected for transitions to the $p1_2$ Rydberg series. We tentatively attribute the absence of such features, which could be observed in H_2, to predissociation.

In accordance with the propensity rule $\Delta N = \Delta l = +1$, observed in the millimeter-wave spectrum of H_2 [18], transitions to the $f1_4[1/2,3/2]$ levels are the most intense. The $n_f f1_4[1/2,3/2] \leftarrow n_i d1_3[1/2,3/2]$ transitions form four line
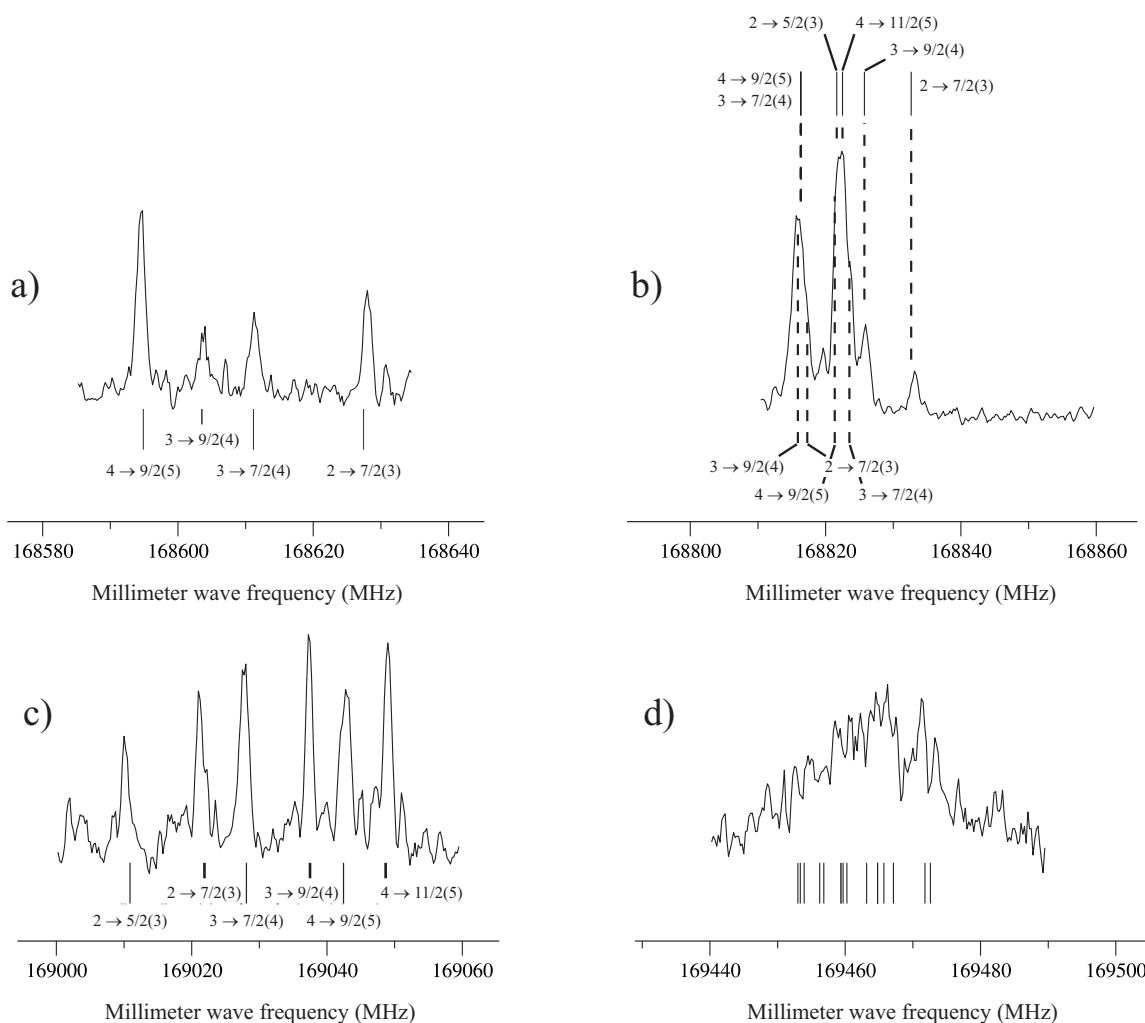
FIG. 5. Panels (a)–(c): Selected regions of the millimeter-wave spectra of the $56f1_4 \leftarrow 52d1_3$ transition with assignment of the hyperfine structure in the notation $F \rightarrow F_s(F)$. (a) Spectral feature associated with the $56f1_4[G^+=1/2] \leftarrow 52d1_3[G^+=3/2]$ transition. (b) Overlapping spectral features associated with the $56f1_4[G^+=3/2] \leftarrow 52d1_3[G^+=3/2]$ and $56f1_4[G^+=1/2] \leftarrow 52d1_3[G^+=1/2]$ transitions. (c) Spectral feature associated with the $56f1_4[G^+=3/2] \leftarrow 52d1_3[G^+=1/2]$ transition. Panel (d): Detail of the spectral feature associated with the $56f1_3[G^+=3/2] \leftarrow 52d1_3[G^+=1/2]$ transition.

clusters, and within each cluster all transitions have the same initial G_i^+ value and the same final G_f^+ value. However, since the interval between the two sets of $G=1$ levels of the d state is almost identical to the interval between the two sets of G_f^+ levels of the f state (approximately 200 MHz), the $G^+=1/2 \rightarrow 1/2$ and $G^+=3/2 \rightarrow 3/2$ features overlap. As n_i changes these two features move slightly relative to one another because the splitting between the two sets of $G=1$ levels varies with n.

The structure of the $n_f f1_4[1/2] \leftarrow n_i d1_3[3/2]$ feature is almost independent of n_i and n_f. In contrast, the linewidths and positions within the $n_f f1_4[3/2] \leftarrow n_i d1_3[1/2]$ feature observed from $n_i=51$ are different from those observed from $n_i=52$ or 53. This observation suggests a perturbation of the $nd1_3[1/2]$ series around $n=51$, potentially by the neighboring $24d3_N$ states (see Fig. 2).

Transitions to the $f1_3[1/2,3/2]$ levels are weaker, broader and less well resolved than transitions to the $f1_4$ levels as a result of lifetime broadening and/or spectral congestion.

The $f1_3[1/2] \leftarrow d1_3[3/2]$ transitions, which are expected to lie in the region of the intense $f1_4[3/2] \leftarrow d1_3[1/2]$ features were not observed. The $f1_3[3/2] \leftarrow d1_3[1/2]$ lines are also very weak, and are not always observed owing to insufficient millimeter-wave intensity. The feature centered at 130 720 MHz in trace (c) has not yet been assigned. Combination differences indicate that these transitions do not form part of the $f1_3[3/2] \leftarrow d1_3[3/2]$ or $f1_3[1/2] \leftarrow d1_3[1/2]$ features.

The variation with frequency of the millimeter-wave power prevented the measurement of transitions in certain ranges, such as the region around 123 200 MHz in trace (e), where transitions to the $f1_2[1/2,3/2]$ levels are expected.

While most spectral structures in Fig. 4 could be fully assigned, the transitions ending on the $f1_2[1/2,3/2]$ levels were too irregular, both in widths and positions, for unambiguous assignments to be made. These transitions were not considered in the analysis.

Panels (a)–(c) in Fig. 5 show the high-resolution millimeter-wave spectra of the $56f1_4[1/2,3/2]$

TABLE I. Observed hyperfine energy levels of the d states of D_2 located below the $X\,^2\Sigma_g^+$ ($v^+=0$, $N^+=1$) ground state of para-D_2^+. The hyperfine levels are labeled using the notation $nlN_N^+(G^+)$, F. All positions are given relative to the position of the $52d1_3(1/2)$, $F=4$ level. $1/\sqrt{W}$ represents the standard deviation in cm^{-1} in the statistical analysis of the combination differences. No value is given when the data set did not contain enough information to derive a standard deviation.

State	F	$E_{\mathrm{obs}}/hc(\mathrm{cm}^{-1})$	$10^{-5}\sqrt{W}$
$51d1_3(3/2)$	2	−1.594959	1.55
$51d1_3(3/2)$	3	−1.594518	5.35
$51d1_3(3/2)$	4	−1.594153	4.47
$52d1_3(1/2)$	4	0.000000	
$52d1_3(1/2)$	3	0.000183	
$52d1_3(1/2)$	2	0.000385	
$52d1_3(3/2)$	2	0.006679	3.45
$52d1_3(3/2)$	3	0.007255	1.70
$52d1_3(3/2)$	4	0.007590	1.36
$53d1_3(1/2)$	4	1.516186	5.08
$53d1_3(1/2)$	3	1.516370	4.47
$53d1_3(1/2)$	2	1.516569	3.66
$53d1_3(3/2)$	2	1.523312	0.70
$53d1_3(3/2)$	3	1.523882	2.36
$53d1_3(3/2)$	4	1.524193	1.18

$\leftarrow 52d1_3[1/2,3/2]$ features, together with the assignment of each of its components in $F[\text{initial}]\rightarrow F_s[\text{final}](F[\text{final}])$ notation. The transitions were assigned using the procedure described in detail in Ref. [18], which relies on the systematic determination of combination differences in conjunction with a comparison of the observed transition patterns with the expected hyperfine structure of the initial and final states (see Fig. 3). The two F components of each F_s level of the f state were not resolved, but an unambiguous assignment of F was made possible by the observation that transitions with $\Delta F=+1$ are favored when $\Delta N=\Delta l=+1$.

The $56f1_3[3/2]\leftarrow 52d1_3[1/2]$ feature is displayed on the same frequency scale in panel (d) of Fig. 5. The expected positions of the transitions which contribute to this feature, as calculated by MQDT using the optimized hyperfine structure of D_2^+ (see Sec. IV), are also indicated. Although individual transitions are not resolved, it is clear that the breadth of the observed feature is consistent with the range of calculated transition frequencies.

To derive a consistent set of relative energies for all of the levels connected by the observed transitions, all transition frequencies and their associated errors were first determined by fitting Gaussian functions to the observed line profiles. Then a least-squares-fitting routine [17] was used to extract the positions of the corresponding d and f states from the transition frequencies, relative to an arbitrarily chosen level, the $52d1_3(1/2)$ level. Because only transitions with $\Delta F=+1$ have been conclusively assigned, f levels with different values of F could not be linked by experimental combination differences. Their relative positions were determined by extrapolating series with different F values to common ionic

levels. Tables I and II list the positions and assignments of all d and f levels determined from the millimeter-wave spectra, respectively. Together with Figs. 4 and 5, these tables represent the main experimental results of the present investigation. The positions of the f levels summarized in Table II were used to derive the hyperfine structure of the ground state of para-D_2^+ by MQDT, as explained in the next section.

IV. COMPARISON WITH MQDT CALCULATIONS AND CONCLUSIONS

MQDT was employed to calculate the positions of the nf levels of D_2 and to determine the hyperfine structure of the ground state of para-D_2^+. The MQDT parameters (i.e., the eigenquantum defect matrix with its dependence on the internuclear separation R and on the energy) were taken from our previous study of the np and nf levels of ortho-H_2 [18] without modification because the eigenquantum defects are expected to be independent of isotopic substitution. The MQDT predictions of Rydberg levels belonging to series converging on the $v^+=0$, $N^+=1$ ionic level are primarily affected by interactions with the $v^+=0$, $N^+=3$ channels and require a precise value for the energy difference between the $N^+=1$ and the $N^+=3$ rotational levels of para-D_2^+. The relative positions of the rovibrational levels of para-D_2^+ were taken from the literature [29,30]. The effects of interactions with vibrationally ($v^+\geq 1$) excited channels were estimated in calculations performed using progressively larger sets of channels, up to $v^+=7$ for the p channels and $v^+=1$ for the f channels. These calculations did not reveal significant perturbations, and we expect that errors in the positions of the corresponding ionic levels used by the MQDT program are of minor importance.

To obtain the hyperfine structure of the $v^+=0$, $N^+=1$ ground state of para-D_2^+ the relative positions of the five hyperfine components were fitted directly to the positions of the f levels listed in Table II. However, to ensure a proper transformation to the actual hyperfine levels of the ion [case e_{exact}, see Eqs. (12)–(21) and Appendixes A and B of Ref. [18]] an approximate estimate of the hyperfine structure is required, which was obtained by scaling the hyperfine structure determined for the $v^+=0$, $N^+=1$ ground state of ortho-H_2^+ using the expressions derived by Carrington $et\ al.$ [28],

$$b_{D_2^+}=\frac{\gamma_d}{\gamma_p}b_{H_2^+}=135.12\ \mathrm{MHz}, \quad (1)$$

$$c_{D_2^+}=\frac{\gamma_d}{\gamma_p}c_{H_2^+}=19.72\ \mathrm{MHz}, \quad (2)$$

$$d_{D_2^+}=\frac{m_{H_2}}{m_{D_2}}d_{H_2^+}=21.21\ \mathrm{MHz}, \quad (3)$$

where $b_{H_2^+}$, $c_{H_2^+}$, and $d_{H_2^+}$ are the main hyperfine structure constants of H_2^+ (see Refs. [18,31]), γ_p and γ_d are the magnetogyric ratios of the proton and deuteron, respectively, and m_{H_2} and m_{D_2} are the masses of H_2 and D_2, respectively. The D_2^+ hyperfine structure calculated using these constants, ne-

TABLE II. Observed and calculated hyperfine energy levels of the f states of D$_2$ located below the $X\,^2\Sigma_g^+$ ($v^+=0$, $N^+=1$) ground state of para-D$_2^+$. The hyperfine levels are labeled using the notation $nlN_N^+(G^+)$, F. All positions are given relative to the position of the $52d1_3(1/2)$, $F=4$ level. $1/\sqrt{W}$ represents the standard deviation in cm^{-1} and W stands for the weight used in the nonlinear MQDT least-squares fit including only $v^+=0$ channels.

State	F	E_{obs}/hc (cm^{-1})	$10^{-5}\sqrt{W}$	Obs.-Calc. (cm^{-1})	State	F	E_{obs}/hc (cm^{-1})	$10^{-5}\sqrt{W}$	Obs.-Calc. (cm^{-1})
$54f1_4(1/2)$	4	2.990691	0.41	0.000071	$56f1_4(1/2)$	4	5.631266	1.60	0.000031
$54f1_4(1/2)$	5	2.990709	1.40	−0.000004	$56f1_4(1/2)$	5	5.631295	1.80	−0.000019
$54f1_4(1/2)$	4	2.990931	1.20	0.000002	$56f1_4(1/2)$	3	5.631505	1.80	0.000013
$54f1_4(1/2)$	3	2.990931	0.36	0.000051	$56f1_4(1/2)$	4	5.631528	2.80	−0.000005
$54f1_4(3/2)$	3	2.997380	1.70	0.000012	$56f1_4(3/2)$	3	5.637961	2.90	−0.000008
$54f1_4(3/2)$	3	2.997735	1.50	0.000026	$56f1_4(3/2)$	3	5.638332	2.40	0.000013
$54f1_4(3/2)$	4	2.997745	0.66	−0.000004	$56f1_4(3/2)$	4	5.638344	2.50	−0.000010
$54f1_4(3/2)$	5	2.998056	1.20	−0.000009	$56f1_4(3/2)$	5	5.638662	2.10	−0.000006
$54f1_4(3/2)$	4	2.998059	2.00	−0.000001	$56f1_4(3/2)$	4	5.638664	3.90	−0.000001
$54f1_4(3/2)$	5	2.998284	2.80	0.000012	$56f1_4(3/2)$	5	5.638871	3.80	0.000000
$55f1_4(1/2)$	4	4.346980	1.50	0.000047	$57f1_4(1/2)$	5	6.848548	1.70	−0.000046
$55f1_4(1/2)$	5	4.347019	1.10	0.000000	$57f1_4(1/2)$	3	6.848770	0.43	−0.000007
$55f1_4(1/2)$	3	4.347235	0.68	0.000043	$57f1_4(1/2)$	4	6.848791	1.40	−0.000023
$55f1_4(1/2)$	4	4.347243	2.00	0.000006	$57f1_4(3/2)$	3	6.855238	1.70	−0.000010
$55f1_4(3/2)$	3	4.353670	3.30	−0.000004	$57f1_4(3/2)$	3	6.855607	1.30	0.000003
$55f1_4(3/2)$	3	4.354037	3.70	0.000017	$57f1_4(3/2)$	4	6.855622	1.40	−0.000013
$55f1_4(3/2)$	4	4.354052	3.30	−0.000005	$57f1_4(3/2)$	5	6.855937	1.20	−0.000013
$55f1_4(3/2)$	5	4.354361	3.40	−0.000011	$57f1_4(3/2)$	4	6.855943	1.30	−0.000004
$55f1_4(3/2)$	4	4.354367	3.90	−0.000001	$57f1_4(3/2)$	5	6.856145	1.90	−0.000005
$55f1_4(3/2)$	5	4.354577	4.20	0.000000					

glecting the role of the nuclear quadrupoles, is displayed in Fig. 6(a). The fitted hyperfine structure of D$_2^+$ determined from the experimental data, shown in Fig. 6(b), was found to be sufficiently similar to this estimate that errors associated with the transformation to the exact ionic levels are expected to be negligible.

The deviations, listed in Table II, between the experimental positions of the nf levels and the positions calculated by
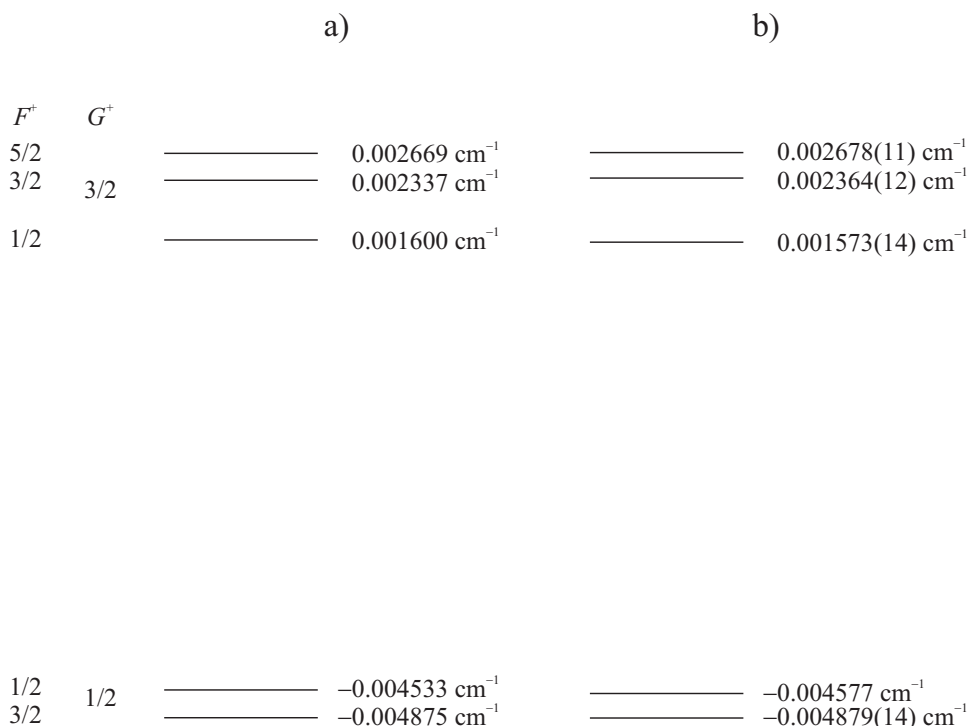
a)   b)

F^+ G^+

5/2 ——————— 0.002669 cm^{-1} ——————— 0.002678(11) cm^{-1}
3/2 3/2 ——————— 0.002337 cm^{-1} ——————— 0.002364(12) cm^{-1}

1/2 ——————— 0.001600 cm^{-1} ——————— 0.001573(14) cm^{-1}

FIG. 6. Hyperfine structure of the $X\,^2\Sigma_g^+$ ($v^+=0$, $N^+=1$) ground state of para-D$_2^+$. (a) Hyperfine structure estimated from the hyperfine structure coupling constants of the $X\,^2\Sigma_g^+$ ($v^+=0$, $N^+=1$) ground state of ortho-H$_2^+$ neglecting the effects of the nuclear quadrupoles. (b) Hyperfine structure determined from the hyperfine structure of the 54–57f Rydberg states in an MQDT fit including only $v^+=0$ channels.

1/2 1/2 ——————— −0.004533 cm^{-1} ——————— −0.004577 cm^{-1}
3/2 ——————— −0.004875 cm^{-1} ——————— −0.004879(14) cm^{-1}

MQDT after optimizing the hyperfine structure of the $v^+=0$, $N^+=1$ state of para-D_2^+ are typically less than 1 MHz (root-mean-square error of 0.000 022 cm^{-1} or $\approx$600 kHz) and are of the same order of magnitude as the deviations obtained in the analysis of the nf levels of H_2 [18]. We therefore believe that the calculations fully explain the experimental results. The normalized root-mean-square error of the fit is 3.0 (a value of 1 would indicate a perfect fit). The large value can be attributed to the facts that (1) the experimental errors used to weigh the transitions are purely statistical and do not include systematic contributions. Although considerable efforts were invested to minimize systematic errors (compensation of stray fields, suppression of power broadening, ac Stark shifts and pressure shifts) we cannot rule out the possibility that the statistical errors give a too optimistic picture of the overall uncertainty, and (2) the MQDT parameters were adopted without adjustment from our previous study of H_2 [18]. An adjustment would undoubtedly have improved the overall quality of the fit, but at the expense of a global description of all isotopomers of molecular hydrogen.

The fitted positions of the hyperfine levels of the $X\,^2\Sigma_g^+$ ($v^+=0$, $N^+=1$) ground state of para-D_2^+ are displayed in Fig. 6(b) where they are compared with the hyperfine structure that was estimated by scaling the hyperfine coupling constants of H_2^+ [see Eqs. (1)–(3)] and neglecting all terms of the hyperfine interaction Hamiltonian that result from the $I=1$ nature of the deuteron [Fig. 6(a)]. These level positions were derived in a direct fit and therefore do not rely on any assumptions concerning the hyperfine Hamiltonian. They could therefore be used to validate future calculations of the hyperfine structure of D_2^+ similar to those presented for H_2^+ [31] and HD$^+$ [32]. The level positions in Fig. 6 are listed with respect to their center of gravity, which would correspond to the position of the $N^+=1$ level of D_2^+ without spin. The position of this level with respect to the lowest $F=5$ nf level observed experimentally ($f1_4[G^+=3/2,F=5]$) is 37.642 971 cm^{-1} (1128.5079 GHz). This interval could be used in a future determination of the adiabatic ionization energy of D_2.

[1] R. S. Mulliken, Phys. Rev. **136**, A962 (1964).

[2] R. S. Mulliken, J. Am. Chem. Soc. **88**, 1849 (1966).

[3] R. S. Mulliken, J. Am. Chem. Soc. **91**, 4615 (1969).

[4] E. Miescher, J. Mol. Spectrosc. **20**, 130 (1966).

[5] E. Miescher and K. P. Huber, in *MPT International review of Science, Physical Chemistry Series 2*, edited by D. A. Ramsay (Butterworths, London, 1976), Vol. 3, p. 37.

[6] G. Herzberg and Ch. Jungen, J. Mol. Spectrosc. **41**, 425 (1972).

[7] P. M. Dehmer and W. A. Chupka, J. Chem. Phys. **65**, 2243 (1976).

[8] M. J. Seaton, Rep. Prog. Phys. **46**, 167 (1983).

[9] U. Fano, Phys. Rev. A **2**, 353 (1970); **15**, 817(E) (1977).

[10] *Molecular Applications of Quantum Defect Theory*, edited by Ch. Jungen (Institute of Physics, Bristol, Philadelphia, 1996).

[11] Ch. Jungen and S. C. Ross, Phys. Rev. A **55**, R2503 (1997).

[12] S. C. Ross and Ch. Jungen, Phys. Rev. A **49**, 4353 (1994).

[13] S. C. Ross and Ch. Jungen, Phys. Rev. A **49**, 4364 (1994).

[14] S. C. Ross and Ch. Jungen, Phys. Rev. A **50**, 4618 (1994).

[15] H. J. Wörner, U. Hollenstein, and F. Merkt, Phys. Rev. A **68**, 032510 (2003).

[16] H. J. Wörner, M. Grütter, E. Vliegen, and F. Merkt, Phys. Rev. A **71**, 052504 (2005); **73**, 059904(E) (2006).

[17] M. Schäfer and F. Merkt, Phys. Rev. A **74**, 062506 (2006).

[18] A. Osterwalder, A. Wüest, F. Merkt, and Ch. Jungen, J. Chem. Phys. **121**, 11810 (2004).

[19] H. J. Wörner, S. Mollet, Ch. Jungen, and F. Merkt, Phys. Rev. A **75**, 062511 (2007).

[20] Ch. Jungen and O. Atabek, J. Chem. Phys. **66**, 5584 (1977).

[21] Ch. Jungen and D. Dill, J. Chem. Phys. **73**, 3338 (1980).

[22] H. Rottke and K. H. Welge, J. Chem. Phys. **97**, 908 (1992).

[23] Th. A. Paul, H. A. Cruse, H. J. Wörner, and F. Merkt, Mol. Phys. **105**, 871 (2007).

[24] A. C. Allison and A. Dalgarno, At. Data **1**, 289 (1969).

[25] NIST Atomic Spectra Database, http://physics.nist.gov/cgi-bin/AtData/main_asd, Version 2.0, 1999.

[26] *MIT Wavelength Tables*, edited by F. M. Phelps III (MIT Press, Cambridge, MA, 1982), Vol. 2.

[27] A. Osterwalder and F. Merkt, Phys. Rev. Lett. **82**, 1831 (1999).

[28] A. Carrington, I. R. McNab, and C. A. Montgomerie, J. Phys. B **22**, 3551 (1989).

[29] Ch. Jungen, I. Dabrowski, G. Herzberg, and M. Vervloet, J. Mol. Spectrosc. **153**, 11 (1992).

[30] L. Wolniewicz and T. Orlikowski, Mol. Phys. **74**, 103 (1991).

[31] J. F. Babb and A. Dalgarno, Phys. Rev. A **46**, R5317 (1992).

[32] D. Bakalov, V. I. Korobov, and S. Schiller, Phys. Rev. Lett. **97**, 243001 (2006).